Water Diffusion and Permeability in Unsaturated Polyester Resin Films Characterized by Measurements Performed with a Water-Specific Permeameter: Analysis of the Transient Permeation

S. MARAIS, M. METAYER, M. LABBE

UMR 6522 "Polymères, Biopolymères et Membranes," Faculté des Sciences, Université de Rouen, 76831 Mont-Saint-Aignan Cedex, France

Received 2 September 1997; accepted 16 April 1999

ABSTRACT: A water-specific permeameter was developed to study water diffusion in an unsaturated polyester; these polyesters are often used as high-barrier materials. Low water enrichment of a dry sweeping gas is measured via the dew point temperature, with two hygrometers, one of which is used because of its fast response and the other because of its accuracy. This high-performance device is just as suited to pervaporation as to permeation tests and allows the transient and stationary fluxes to be characterized. At first sight, the experimental data seem in good agreement with $D = D_0 e^{\gamma C}$. However, a more thorough study has shown a time-dependence of D. © 1999 John Wiley & Sons, Inc. J Appl Polym Sci 74: 3380–3395, 1999

Key words: unsaturated polyester resin; water diffusion in polymers; water-specific permeameter; plasticization

INTRODUCTION

Because of their favorable performance as high-barrier materials, dense polymers characterized by very low water permeabilities are extensively used in the automobile, military, space, and naval industries, as well as in the building trade and in electronics. The first resins to appear, unsaturated polyester resins (UPRs), have decreased in cost and their characteristics are well documented; ninety-five percent of their use is in fiber-reinforced composite systems.

Fiber-reinforced plastic composite materials are increasingly in demand where resistance to chemical environments is paramount. In the naval industries, for example, UPRs can be used as gel coats, but are more often reinforced with fibers and used for boat hulls.

However, the reaction of these crosslinked polyester resins with water leads to aging. Water diffusion through the resins can cause reversible phenomena such as plasticization and local strain, but also irreversible modification such as chain rupture and chemical degradation, which then contribute further to the aging of the material.[1] It is not surprising, therefore, that there is currently much interest in the problem of water diffusion and permeability in tridimensional polymers.

Various techniques are available to determine the water diffusivity and permeability in polymer films: The principal techniques used are sorption and vapor-transmission measurements. Sorption kinetics are usually carried out by weighing methods which are not specific to water (because of other volatile substances) and often require expensive equipment, in particular, an insulated and very sensitive microbalance.

For these reasons, we have preferred to build and to perfect a water-specific permeameter. This

Correspondence to: M. Metayer.

Journal of Applied Polymer Science, Vol. 74, 3380–3395 (1999)
 CCC 0021-8995/99/143380-16

consists of a vapor-transmission cell divided into two chambers by the film tested. One of the chambers is either in contact with pure liquid water (pervaporation) or swept with a gas rich in relative humidity (RH) (permeation). The other chamber is maintained at very low RH by circulating a dry sweeping gas through it. In a previous study,[2] water-transient fluxes through UPR films were monitored versus time, but the sensor used only allowed relative measurements. Later, a time-lag diffusion coefficient D_ℓ was determined. The experimental flux curves were consistent with a nonconstant diffusion coefficient (increasing with concentration). Since then, the permeameter has been equipped with a hygrometric unit which reconciles a fast-response time and accuracy of absolute measurements. The high sensitivity of the water sensor allows the transient and steady states of permeation to be analyzed in order to determine the diffusivity and permeability to water, but also to emphasize a possible deviation from Fickian behavior, which can be due, for example, to a plasticization phenomenon.

In this article, we show, through an original experimental method, a high-performance process to characterize water diffusion in polymer films and, particularly, in dense polymers with very low water permeabilities. Pervaporation and permeation through a commercial crosslinked polyester resin were measured.

EXPERIMENTAL

Pervaporation and permeation tests were performed on an unsaturated crosslinked polyester resin provided by Technibat Co.* Using original high-performance equipment, this process calculates more accurate flow density throughout the test from zero time to the steady-state plateau. Thus, the water diffusivity is obtained from the transient regime, and the permeability of the polymer films, from the steady state.

Materials

The selected UPR consists of maleic anhydride (25% mol), isophtalic acid (25% mol), and propylene glycol (50% mol) mixed in a styrene monomer solution (38% w/w). Films are prepared by mixing this resin first with a solution of cobalt octoate [the promotor (0.2% w/w)] and then with a methyl ethyl ketone peroxide [the initiator MEKP, Akzo, Compiegne, France (1.5% w/w)]. The resin is then cast between two polypropylene plates for 24 h at room temperature and postcured at 80°C for 6 h and at 120°C for 2 h.

Water-specific Permeameter

An experimental device was perfected. It consists of a measurement cell, a supply of gas (nitrogen is used as sweeping dry gas), and a hygrometric unit connected to an acquisition system. This hygrometric unit consists of two devices. One was selected because of its fast response (Shaw hygrometer, Gruter & Marchand†), and the other, for its accuracy (chilled mirror hygrometer, General Eastern)‡.

Measurement Cell

The measurement cell consists of two compartments separated by the polymer film. The upper compartment (upstream) is supplied with liquid or vapor water (pervaporation or permeation). The lower compartment (downstream) is swept with the dry gas. The capacitive probe (Shaw hygrometer) is placed inside the receiving chamber outlet. The mirror hygrometer is connected in series. Pervaporation and permeation tests are performed with two slightly different cells. The receiving compartment, which is the same in both cases, allows measurements in similar conditions.

The downstream half-cell is common to pervaporation and permeation [Fig. 1(b)]. It consists of a receiving chamber with the following dimensions: 10 cm (length) × 3 cm (width) × 0.1 cm (depth). It is made of 316 L stainless steel and is thick enough not to be deformed when the two parts are tightened.

The upstream half-cell for pervaporation is a source compartment supplied with liquid water (volume = $10 \times 3 \times 0.4$ cm^3) [Fig. 1(a)]. It is made of transparent Plexiglas so that the rate of filling with liquid water (in the chamber) and the homogeneous distribution of water on the polymer surface can be correctly monitored and controlled.

* Technibat Co., manufacturer of products based on polyester resins, taken over by Cray-Valley (Total) in 1996, Z.I. Gravigny, 27002 Cedex France.

† Gruter & Marchand, manufacturer of SHAW hygrometer, F-92000 Nanterre, France.

‡ General Eastern, manufacturer of chilled mirror hygrometer, Woburn, MA.

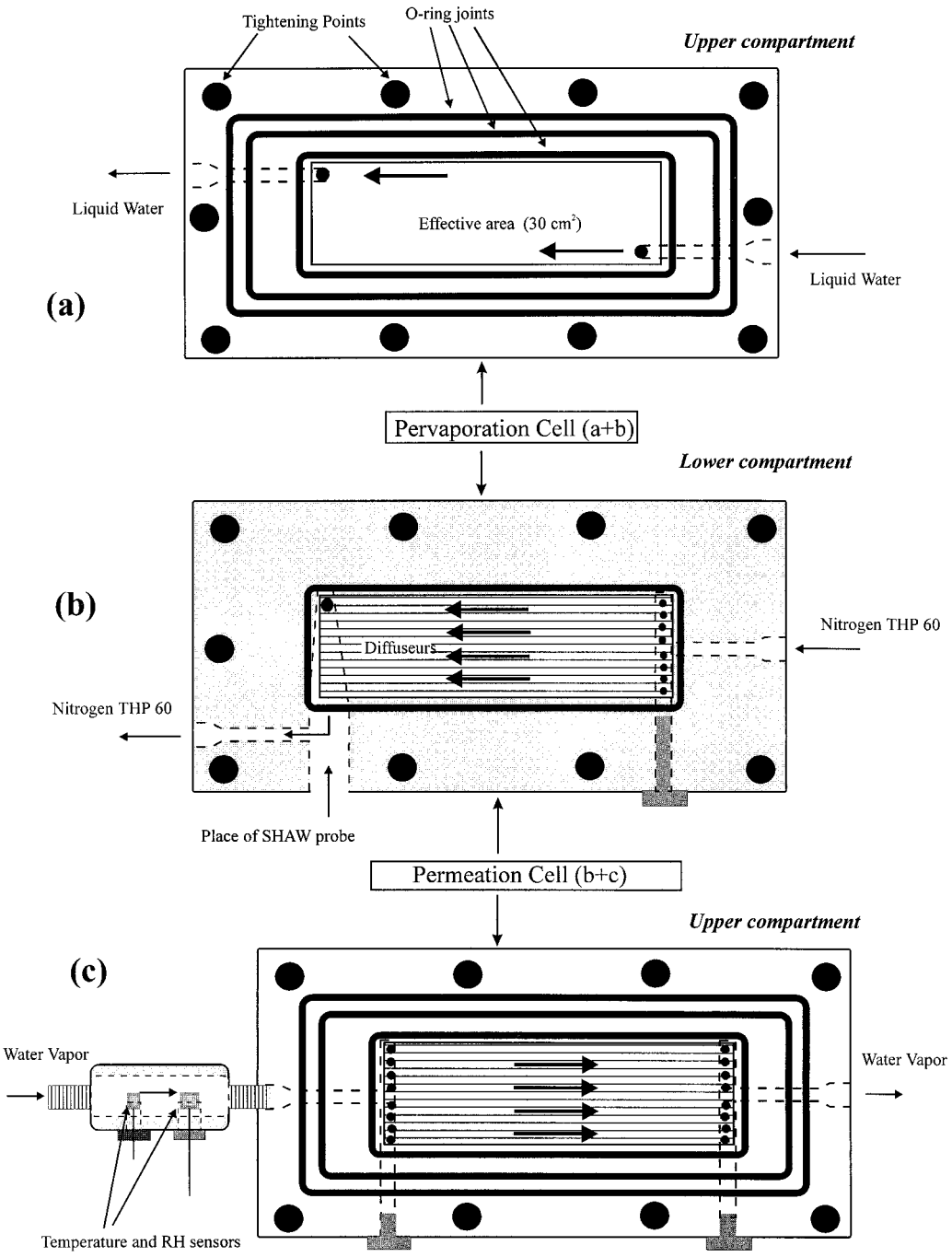

Figure 1 Measurement cell: (a) upstream half-cell for pervaporation; (b) downstream half-cell for pervaporation and permeation; (c) upstream half-cell for permeation.

The upstream half-cell for vapor permeation is a source compartment supplied with a wet gas (volume = $10 \times 3 \times 0.2$ cm^3) [Fig. 1(c)]. It is also made of transparent Plexiglas to visualize the position of the polymer film and to detect possible condensation, which must be avoided. The vapor pressure is controlled and regulated inside the chamber by two sensors, temperature and RH, connected to the acquisition system.

Fluids

In both cases, the compartments are made water-tight with O-ring joints. Each compartment has

Table I THP 6.0 Quality Nitrogen Characteristics

N_2	$\geq$ 99.9999%
H_2O	$<$ 0.6 ppm V
O_2	$<$ 0.1 ppm V
CO	$<$ 0.1 ppm V
H_2	$<$ 0.1 ppm V
CO_2	$<$ 0.05 ppm V
C_nH_m	$<$ 0.01 ppm V

been designed to ensure a good distribution of fluids (gas and water vapor) on both sides of the film.

A drying step comes before water-transmission measurement and requires each compartment to be swept with dry gas. The lower compartment is supplied with ultradry nitrogen (THP 60 from Carboxyque Francaise, F76530 Grand-Couronne, France; see Table I) and has a very low stabilized concentration of water, thus ensuring a high sensitivity of the water-flow measurements.

During the preliminary step, the upper compartment is supplied with I nitrogen (Air Liquid, F76303 Sotteville les Rouen, France; see Table II) whose moisture content is sufficiently low to achieve drying of the film before the start of the pervaporation or permeation test. When the film is dry, the gas is replaced with ultrapure water (Milli-Q Water System, resistivity 18/cm) for the pervaporation test or water vapor in nitrogen for the permeation test. The humidity of this gas is adjusted by mixing it with dry nitrogen.

Hygrometers

Shaw Hygrometer. A multichannel system was equipped with a "red-point" probe which is used in the range −80°C/−20°C of the dew point (see Table III). This probe consists of an electric condenser made of an aluminum wire (high purity) covered with a 10-μm (thin) aluminum oxide layer (hygroscopic) and a porous gold film. Some water-vapor molecules around the probe diffuse through the dielectric layer, and owing to the extremely thin micropores, vapor water is condensed; because of the very high dielectric constant of water (80), there is a variation of the dielectric value of the probe. An equilibrium occurs between the water vapor around the probe and the condensed water in the micropores of the oxide layer. This equilibrium is maintained and the response time of the probe is generally short (30 s for dry values to wet values). The variation of the capacity is proportional to the dew point temperature, and the signal, which is a linear function of the dew point in the range −75°C/−20°C, is transmitted via the hygrometer to a data aquisition control unit (14-bit AD/DA card) equipped with specific software. According to the manufacturer, the precision and the reliability are, respectively, 3°C or 1 ppm V and 0.5°C or 0.2 ppm V, respectively.

Table II *I* Quality Nitrogen Characteristics

N_2	$\geq$ 99.8%
H_2O	$<$ 10 ppm V
O_2	$<$ 10 ppm V

Table III Red Point SHAW Probe Characteristics

Measurement range	−80 to +20°C T_{dp} 0–1000 ppm V
Working temperature	−35 to +40°C
Linear response	4°C
Accuracy	±3°C T_{dp}

Chilled Mirror Hygrometer. This type of hygrometer measures the exact water-vapor concentration of a gas by direct measurement of its dew point. Indeed, this apparatus is usually used as a reference for humidity measurements. For our tests of low water permeability, we used the General Eastern M4DP model equipped with the 1311DR sensor (see Table IV). The probe signal is a linear function of the dew point temperature in the range −80°C/+20°C. The 1311DR is a stainless-steel, liquid-cooled, four-stage sensor. Optical condensation hygrometry is a precise technique for determining the water-vapor content in gases by measuring dew or frost temperatures.

Table IV Chilled Mirror Sensor Characteristics

Measurement range (Dew point)	−65 to +20°C, air −80 to +20°C, liq.
Accuracy	±0.2°C
Reliability	±0.05°C
Cooling stages	4
Operating ranges	
Ambient temperature	0 to +35°C
Pressure (psig)	0 to +300

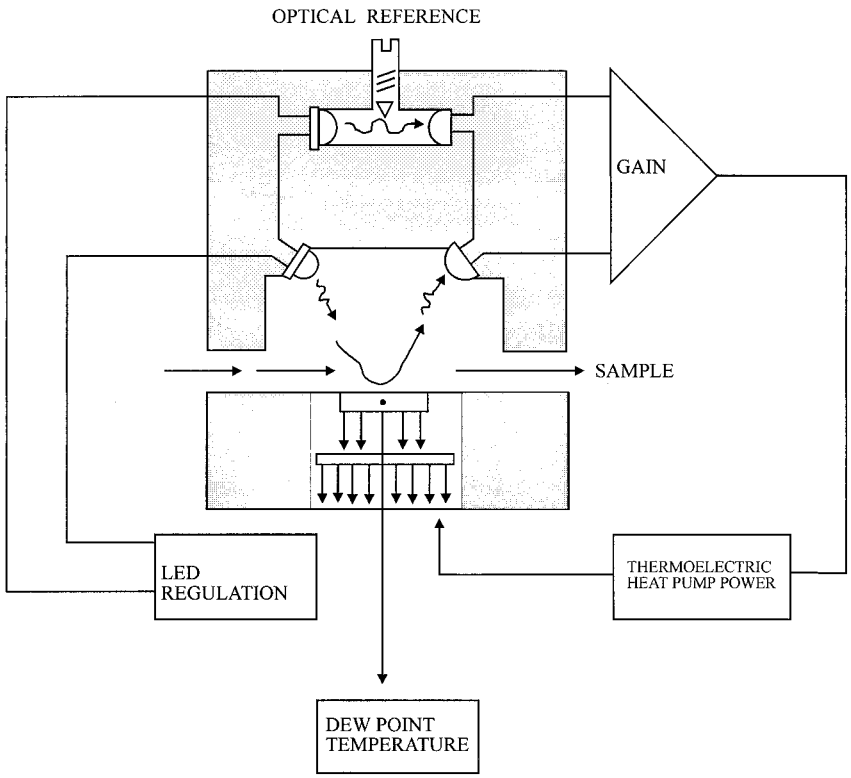

Figure 2 Chilled mirror sensor block diagram.

Because these hygrometers are so accurate (0.2°C for this model), they are widely used as a standard in many of the world's metrology laboratories. A metallic mirror surface is cooled until it reaches a temperature at which condensation begins to form on it. The dew layer is optically detected and the mirror is held at that temperature. The mirror temperature, measured with a platinum resistance thermometer, is an accurate indicator of the dew or frost point. Figure 2 illustrates the way in which this chilled mirror hygrometer detects and measures the dew point. The response time, which is about a few seconds at dew points above 0°C, slows to a few minutes below −60°C. The manufacturer gives the precision and the fidelity as, respectively, 0.2°C dew points or 0.07 ppm V and 0.05°C or 0.02 ppm V, respectively. All the parts of the experimental device sensitive to temperature are arranged in a chamber maintained at constant temperature (e.g., 25°C).

Experimental Procedure

The thermoregulated chamber is adjusted to the desired temperature. The film sample thickness is measured using a ROCH 0-25 micrometer (see Table V) on 21 points (3 × 7, evenly distributed). The film sample is stored in a desiccator under a full vacuum for 12 h at room temperature, then inserted into the cell. The compartments are screwed together in order to obtain a regular tightening. Figure 3 shows the experimental setup of pervaporation [Fig. 3(a)] and permeation [Fig. 3(b)].

In this study, all the measurements were carried out at 25°C. They relate to a single film which has the following characteristics: thickness $L = (0.028 \pm 0.005)$ cm, exposed area $S = 30$ cm^2, and voluminal mass $\rho = 1.15$ g cm^{-3}.

Preliminary Drying

Valves 1 (I nitrogen) and 2 (THP60 nitrogen) (see Fig. 3) are opened and their flow rates adjusted to

Table V ROCH 0–25 Micrometer Characteristics

Error	1 μm
Reference temperature	20°C
Parallelism	0.9

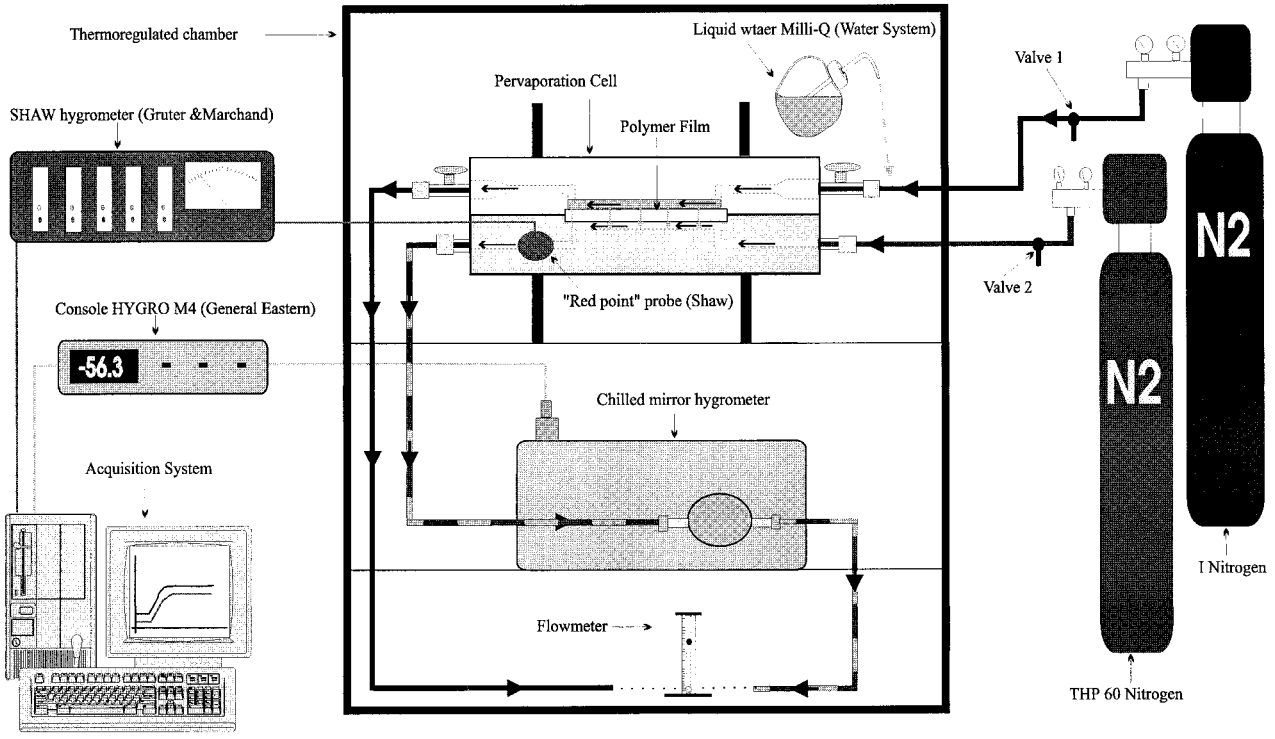

a

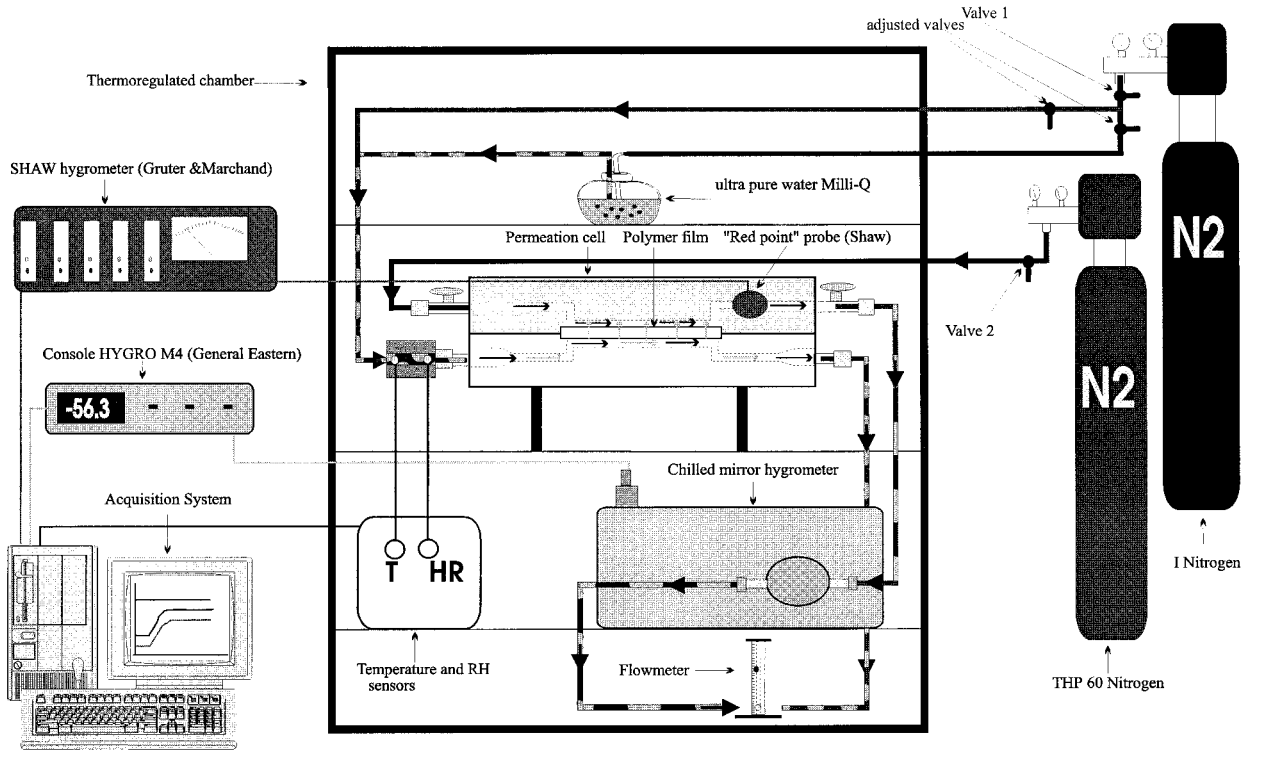

b

Figure 3 Experimental setup: (a) pervaporation; (b) permeation.

3.5 $cm^3\ s^{-1}$ for the first 10 h of drying. In the second step, the flow rates must increase up to 9.3 $cm^3\ s^{-1}$: To obtain a fast-response time from the chilled mirror hygrometer, the sweeping gas flow must be used between 3.3 $cm^3\ s^{-1}$ and 41.7 $cm^3\ s^{-1}$. The gas flow of 9.3 $cm^3\ s^{-1}$ represents an optimal flow which offers a good compromise of a sufficient flow for measurements (time response) without consuming too much gas (high-purity nitrogen). Valve 1 can be closed only when the probe signal is stabilized, indicating that the humidity of the gas leaving the cell has reached a plateau ($-75°C < T_{dp} < -70°C$).

The Pervaporation Test [Fig. 3(a)]

The upstream compartment is quickly filled with pure water or saturated saline solutions (water activity: $a_h = 1$ with pure water, and $a_h = 0.58$ with NaBr). The time taken is negligible and so without significant influence on the zero-time determination. Then, the transfer of water through the film from the upstream to the downstream compartment can be monitored by using the signals of the humidity sensors which follow the increase of water vapor in the sweeping gas.

The Permeation Test [Fig. 3(b)]

The upstream compartment is quickly filled with water vapor obtained by an adjusted mixture of dry gas (I nitrogen) and humid gas (I nitrogen circulating in a water-bubble chamber) at the desired RH and controlled with temperature and RH sensors. The same film used for pervaporation measurements was tested in permeation by supplying the source side with 95 and 58% RH (a_h = 0.95 and 0.58).

THEORY

Permeation is studied through a film of thickness L and of exposed area S. Its upstream face, located at $x = 0$, is in contact with pure water or with a gaseous phase in which water vapor is at constant pressure p_h. The downstream face, at $x = L$, is swept with a dry gas whose flow rate f is adjusted to ensure low vapor pressure p_{out} in the effluent gas. On the assumption of local equilibrium, interfacial concentration of sorbed water is kept constant when $x = 0$ or negligible when $x = L$. Initially, the film is free from water.

Concentration and flux profiles, $C(x,t)$ and $J(x,t)$, are described by Fick's laws and boundary conditions[3]:

$$J(x, t) = -D \frac{\partial C(x, t)}{\partial x} \tag{1}$$

$$\frac{\partial C(x, t)}{\partial t} = -\frac{\partial J(x, t)}{\partial x} \tag{2}$$

$$C(0, t) = C_h \text{ (constant)} \quad \text{and} \quad C(L, t) \approx 0, \ \forall\, t \tag{3}$$

$$C(x, t) = 0, \quad \forall\, 0 < x < L, \quad t = 0 \tag{4}$$

D is the diffusion coefficient of water in the film.

These equations give the flux $J(L,t)$ at the downstream interface and the quantity of water Q which passes through the interface and accumulates in the receiving chamber during the period of diffusion t:

$$J(L, t) = -D\left[\frac{\partial C(x, t)}{\partial x}\right]_{x=L} \tag{5}$$

$$Q = S \int_{t=0}^{t} J(L, t)dt \tag{6}$$

After a latent time, $J(L,t)$ increases progressively up to a limit J_{st} typical of the steady state. When the water content is assumed to be nil at the downstream interface,

$$J_{st} = \frac{\bar{D} C_h}{L} \tag{7}$$

with

$$\bar{D} = \frac{1}{C_h} \int_0^{C_h} D dC \tag{8}$$

the integral diffusion coefficient.

Unlike C_h, water activity a_h at the upstream interface is known, and a permeability coefficient P can be defined as

$$P = \frac{J_{st} L}{a_h} \tag{9}$$

with P expressed in mmol cm^{-1} s^{-1}. In pervaporation with pure water, $a_h = 1$. In permeation, $a_h = p_h/p_{st}$, where p_h and p_{st} are vapor and saturated vapor pressures, respectively.§

Usually, C_h is related to a_h via a solubility coefficient σ:

$$C_h = \sigma a_h \tag{10}$$

A time-lag diffusion coefficient D_l value can be obtained from

$$D_\ell = \frac{L^2}{6t_\ell} \tag{11}$$

knowing that t_ℓ is the intercept on the time axis of the asymptotic line of the curve $Q = f(t)$.[3] A more complex relation for the concentration-dependent time lag was obtained by Frisch[4] without explicitly solving the diffusion equations:

$$t_\ell = \frac{L^2\left\{\int_0^{C_h} wD(w)\left[\int_w^{C_h} D(u)du\right]dw\right\}}{\left[\int_0^{C_h} D(u)du\right]^3} \tag{12}$$

To highlight a concentration-dependent diffusion coefficient, the shape of the experimental curve $J = f(t)$, rather than $Q = f(t)$, can be analyzed. The particular case of D constant is characterized by a reduced curve $j = f(\tau)$ with $j = J/J_{st}$ and $\tau = Dt/L^2$:

$$j = \frac{2}{\sqrt{\pi\tau}}\left[\sum_{n=0}^{\infty} e^{-(2n+1)^2/4\tau}\right] \tag{13a}$$

$$j = 1 + 2\sum_{n=1}^{\infty}(-1)^n e^{(-n^2\pi^2\tau)} \tag{13b}$$

Equation (13a) or (13b) can be limited to $n = 2$ for $\tau < 0.3$ or $\tau > 0.2$, respectively. This reduced curve $j = f(\tau)$ shows an inflexion point $R(\tau_R = 0.091, j_R = 0.24)$; see Figure 4(a) or (b) with $\tau = \tau_0$ or $<\tau>$ and $\gamma C_h = 0$.

§ Usually P is defined as P equals $J_{ST}\,L/p_h$ and expressed in cm^3 (STP) cm^{-1} s^{-1} cmHg^{-1}.

When D depends on concentration, the reduced time τ_0 can be defined from the diffusion coefficient D_0 at zero concentration:

$$\tau_0 = \frac{D_0 t}{L^2} \tag{14a}$$

A time $t = t_R$, for which $j = j_R = 0.24$, τ_0 is denoted

$$\tau_{0,R} = \frac{D_0 t_R}{L^2} \tag{14b}$$

An alternative dimensionless time $<\tau>$ can be chosen as

$$\langle\tau\rangle = \frac{\tau_R t}{t_R} \tag{15}$$

so that the curve $\tau = f(<\tau>)$ passes through R. At this point, the slope

$$\alpha = \left[\frac{\Delta j}{\Delta t}\right]_{\tau=tR} \tag{16}$$

depends on the D variation law. When D is constant, increases, or decreases with concentration, $\alpha = \alpha_0 = 5.82$, $\alpha > \alpha_0$ or $\alpha < \alpha_0$. The slope α could be used as a significant parameter of the concentration dependence.

RESULTS AND DISCUSSION

Dew Point of Sweeping Gas and Water Flux

The downstream chamber is supplied with a carrier gas, at flow-rate $f = 9.3$ cm^3 s^{-1} (optimal flow necessary for using a mirror hygrometer) at total pressure $p_t = 1$ atm. This gas is not strictly free from water and the water-vapor pressure increases from p^{in} up to p^{out} (Fig. 5), so that the flux $J(L,t)$ is

$$J(L,\,t) = \frac{f}{S}\frac{p^{out} - p^{in}}{RT_R} \tag{17}$$

with R the gas constant and T_R the temperature (K) of the experiment (room temperature). Pressures p^{in} and p^{out} are indirectly obtained from the dew points T_{dp} of the carrier gas, according to the well-known Clapeyron–Clausius relation:

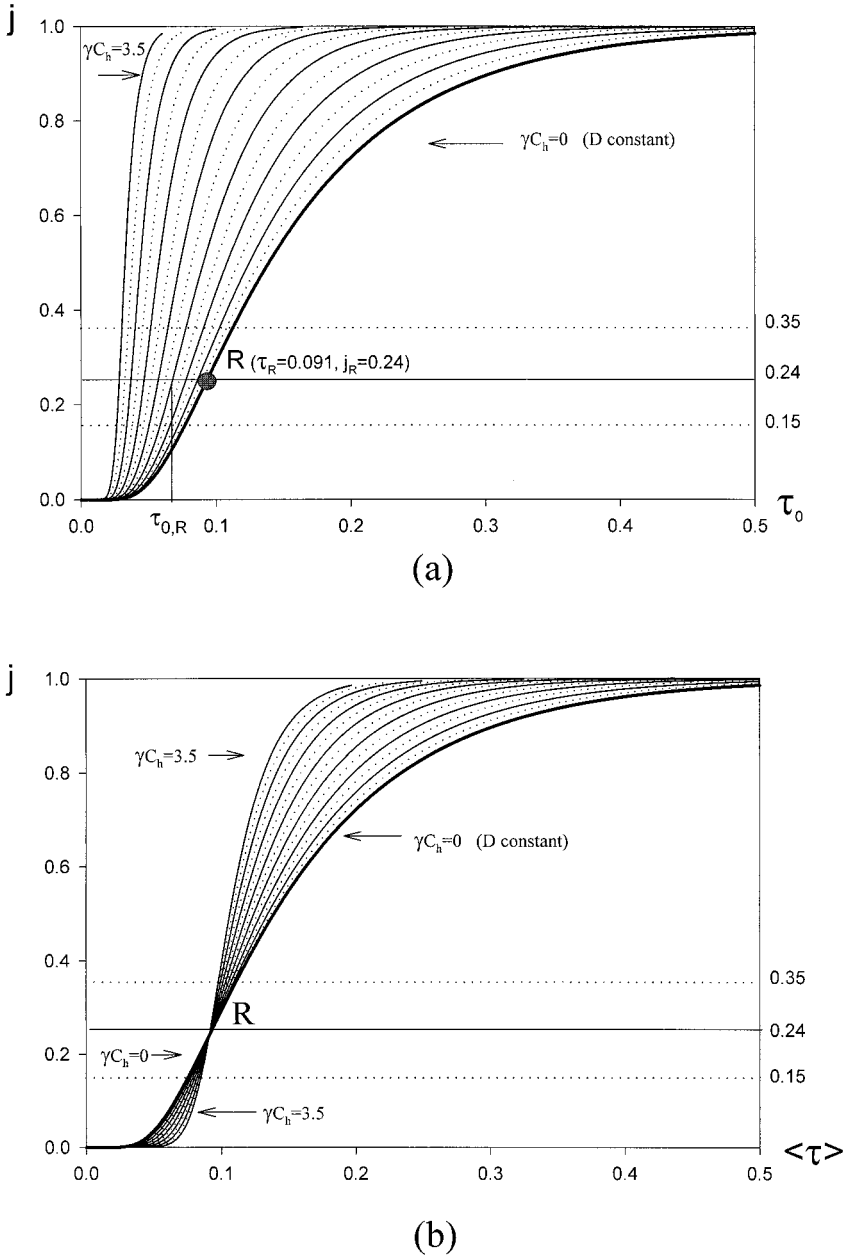

Figure 4 Theoretical flux j versus time for various values of γC_h when $D = D_0 e^{\gamma C}$. Reduced scales with (a) $\tau_0 = D_0 t/L^2$ [eq. (14a) or (14b)] or (b) $<\tau> = \tau_0\ \tau_R/\tau_{0,R}$. $\tau_R = 0.091$ and $j_R = 0.24$ are the coordinates of point R in both figures.

$$\frac{dLnp_{st}}{d(1/T)} = -\frac{\Delta H_v(T)}{R} \tag{18}$$

with $\Delta H_v(T)$, the vaporization enthalpy at temperature T. Provided that $\Delta H_v(T)$ is constant:

$$p = \exp\left(-\frac{A}{T_{dp}} + B\right) \quad \text{at temperature } T_R \tag{19}$$

Knowing that p becomes p_{st} when $T_R = T_{dp}$, ppm V concentration x can be used instead of pressure p (x ppm V = $10^6 \cdot p/p_t$, p_t is the total pressure), so that

$$J(L, t) = \frac{273.15}{22.4}\frac{f\ 10^{-6}(x^{out} - x^{in})}{ST_R} \tag{20}$$

with

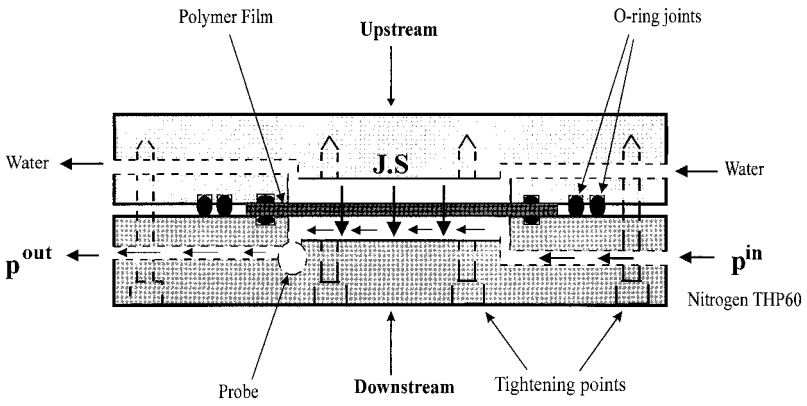

Figure 5 Water-vapor pressure at the inlet (p^{in}) and at the outlet (p^{out}) of the measurement cell.

$$x = \exp\left(-\frac{6185.66}{T_{dp}} + 31.38\right) \qquad (21)$$

in the dew point range −70 to −50°C.[5]

Permeation Tests (Pervaporation and Vapor Permeation)

Experimental Curves

Experimentally, the increasing of the dew point of the carrier gas (which corresponds to the enrichment of water concentration) is monitored as a function of time up to the steady state with a chosen frequency of one point every 10 s (Fig. 6). Figure 6(a) shows the values displayed by both hygrometers, and Figure 6(b) shows both smoothed curves which have a sigmoidal shape.[6]

Differences between both curves are explained by the hygrometer characteristics. The mirror hygrometer gives two accurate dew points, below 1 h M_0 and above 6 h M_{st}, which are used to adjust the "Shaw curve." Figure 6(c), therefore, benefits from the qualities of each hygrometer: the fast-response of the Shaw (for the transient step) and the accuracy of the Mirror (for the start and the steady state).

From these data, the experimental flux J_{exp} and the accumulated quantity Q_{exp} are calculated from eqs. (20), (21), and (6) and plotted against time (Fig. 7). The permeability coefficient P is deduced from J_{st} and eq. (9) (see Table VI). The reduced curve $j = f(<\tau>)$ is drawn using $<\tau>$ given by eq. (15). The slope α, given by eq. (15), is thus obtained. Its value, which is higher than α_0 (see Table VI) agrees with a diffusion coefficient increasing with concentration. For this reason, we have chosen the following law[7]:

$$D = D_0 e^{\gamma C} \qquad (22)$$

which, from ref. 8, can be applied to glassy polymers, knowing that γ could be a measure of water-induced depression of the polymer glass transition.[9]

Computed Curves

It is always possible to compute j by solving eqs. (1)–(4) numerically. The following reduced parameters:

$$\tilde{C} = C/C_h$$

$$\tilde{D} = D/D_0$$

$$\tilde{\gamma} = \gamma C_h$$

$$\tilde{x} = x/L \qquad (23)$$

are used in addition to τ_0 and $j = J/J_{st}$. The boundary conditions [eqs. (3) and (4) become

$$\tilde{C}(0, \tau_0) = 1 \quad \text{and} \quad \tilde{C}(1, \tau_0) \approx 0 \; \forall \; \tau_0$$

$$\tilde{C}(\tilde{x}, \tau_0) = 0 \; \forall \; 0 < \tilde{x} < 1, \quad \tau_0 = 0 \qquad (24)$$

The diffusion coefficient is assumed to increase with concentration according to eq. (22):

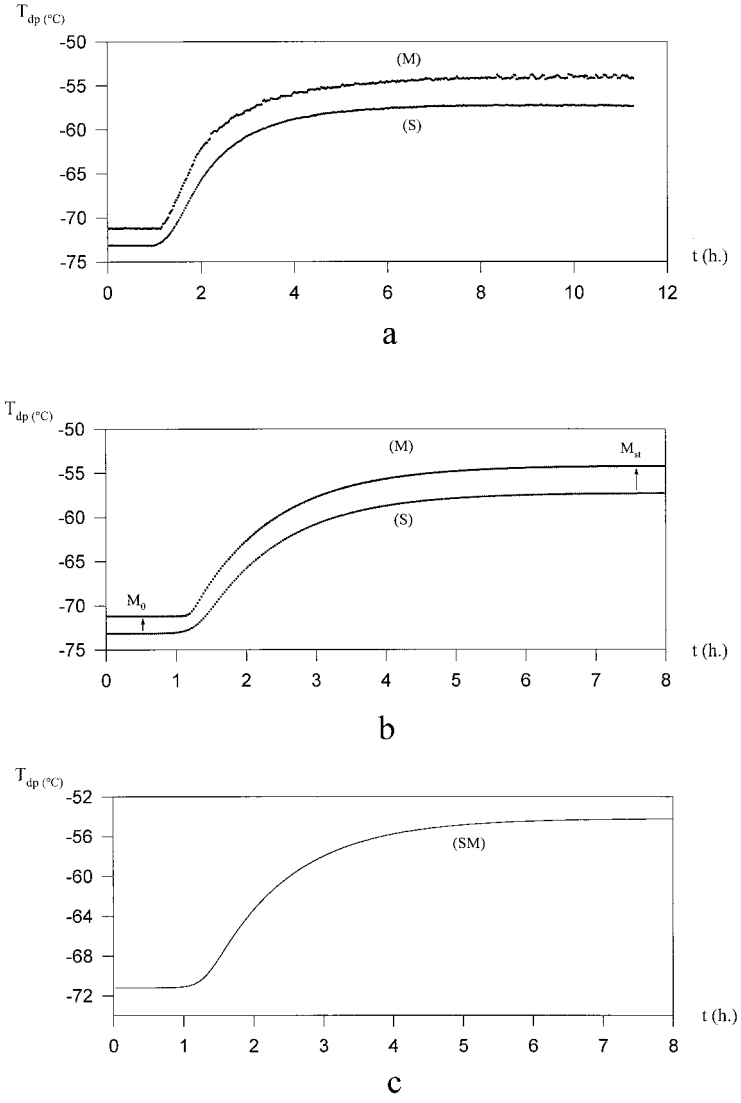

Figure 6 Recording of dew point versus time of mirror (M) and Shaw (S) hygrometers (pervaporation no. 1): (a) unsmoothed signals; (b) smoothed signals with M_0 and M_{st} reference dew points from the mirror; (c) Shaw curve adjusted from M_0 and M_{st}.

$$\tilde{D} = e^{\tilde{\gamma}\tilde{C}} \tag{25}$$

Equations (1)–(4) are worked out from the finite difference method by using constant increments, with the stability criterion

$$r = \frac{\Delta\tau_0}{(\Delta\tilde{x})^2} \leq e^{-\tilde{\gamma}}/2 \tag{26}$$

in place of $r \leq 1/2$, when D is constant.[10]

Curves $j = f(\tau_0)$ are drawn for various values of $\tilde{\gamma}$ [cf. Fig. 4(a)]. When $\tilde{\gamma} = 0$ ($D = D_0$, constant), the curve $j = f(\tau)$ passes through the characteristic point R ($\tau_R = 0.091, j_R = 0.24$). In other cases, the time $\tau_{0,R}$ (at $j = j_R$) is determined as a function of $\tilde{\gamma}$. In agreement with eqs. 14(a) and (b), the change of the time scale

$$\langle\tau\rangle = \frac{\tau_0\tau_R}{\tau_{0,R}} \tag{27}$$

gives a set of curves which intersect at point R [cf. Fig. 4(b)], each curve being characterized by a slope α . All the curves presented in Figure 4 depend on $\tilde{\gamma}$ alone. The resulting relations between $\tilde{\gamma}$ and α, then $\tau_{0,R}$, and $\tilde{\gamma}$ are shown in Figure 8(a,b).

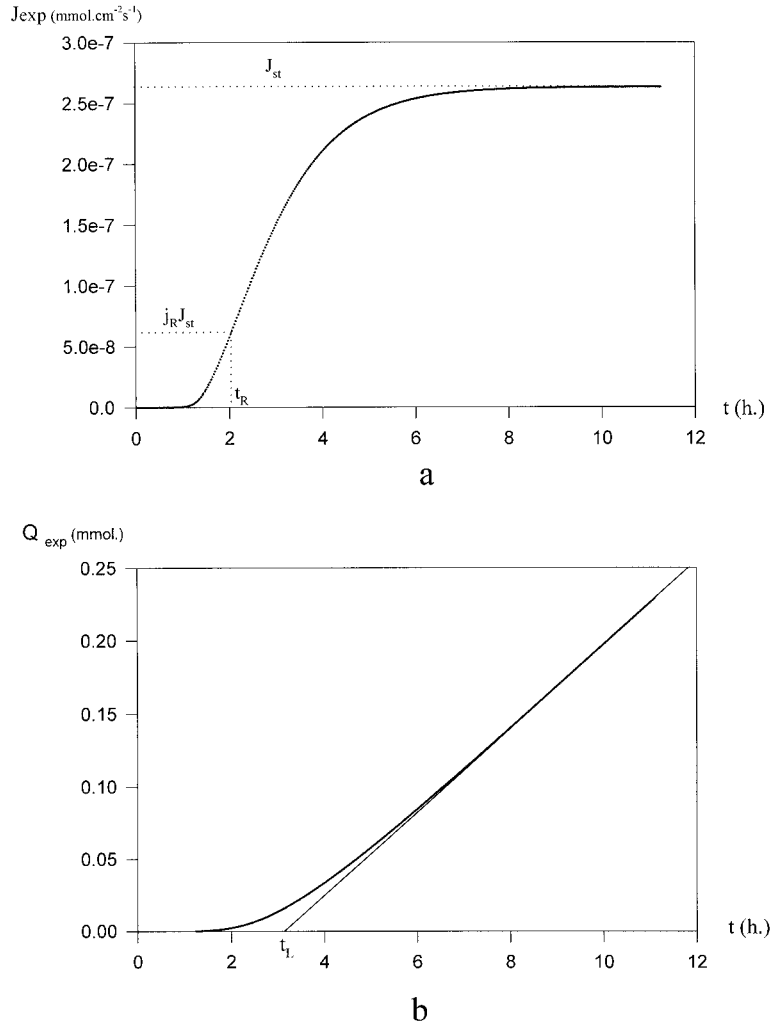

Figure 7 (a) Experimental water flux J_{exp} and (b) its integration Q_{exp} versus time.

Data Treatment

The time t_R is obtained from the experimental curve $J = f(t)$, as shown in Figure 7(a), by using the least-squares line in the range $0.15 < j < 0.35$ (in accordance with Fig. 4). The values of t_R and J_{st} allow both reduced parameters $<\tau>$, from eq. (15), and $j = J/J_{st}$ to be defined, and the slope α on curve $j = f(<\tau>)$ can then be calculated as defined from eq. (16).

Figure 8(a,b) links $\tilde{\gamma}$ and $\tau_{0,R}$. From these relations, $\gamma C_h = \tilde{\gamma}$ and $D_0 = \tau_{0,R} L^2/t_R$ are deduced. The curve computed from these two parameters is drawn and compared with the experimental data (see Fig. 9). An excellent agreement is obtained, which seems to justify the law that $D = D_0 e^{\gamma C}$.

The experimental data in Figures 7(a) and 9 correspond to the test Pervaporation no. 1 in Table VI, with $a_h = 1$. In this case, it can be deduced that $\gamma C_h = 1.71$ and that the diffusion coefficient D varies from $D_0 = 0.65 \times 10^{-8}$ cm^2 s^{-1} ($C = 0$ downstream) up to $D_M = D_0 e^{\gamma C} h = 3.6 \times 10^{-8}$ cm^2 s^{-1} ($C = C_h$ upstream). The other parameters in Table VI were obtained as

$$P = \frac{J_{st} L}{a_h}, \quad \text{from eq. (9)} \tag{28}$$

$$\gamma = \frac{D_M - D_0}{J_{st} L}, \quad \text{with } D_M = D_0 e^{\gamma C_h} \text{ from eqs. (7), (8) and (22)} \tag{29}$$

$$\sigma = \frac{C_h}{a_h}, \quad \text{with } C_h = \frac{\bar{\gamma}}{\gamma}, \text{ from eqs. (10) and (23)} \tag{30}$$

Table VI Characteristic Parameters from Pervaporation and Permeation

Test	a_0	$P \times 10^9$	α	γC_h	γ	σ	D_ℓ	$D_0 \times 10^8$	$\bar{D} \times 10^8$
Pervaporation no. 1	1	7.3 ± 1.2	8.3	1.71	4.05	0.42	1.17	0.65	1.7
Pervaporation no. 2	1	7.3 ± 1.2	8.3	1.74	4.10	0.42	1.16	0.64	1.7
Pervaporation no. 3	0.58	4.9 ± 0.8	8.1	1.66	9.08	0.32	1.03	0.60	1.5
Permeation no. 1	0.95	6.3 ± 1.1	7.5	1.35	3.93	0.36	1.23	0.82	1.7
Permeation no. 2	0.58	6.1 ± 1.1	8.0	1.58	7.50	0.36	1.11	0.69	1.7

P in mmol cm^{-1} s^{-1}; D_ℓ, D_0, and $\bar{D}$ in cm^2 s^{-1}; γ in cm^3 mmol^{-1} and σ in mmol cm^{-3}. Pervaporation nos. 1 and 2 repeat the same test of pervaporation.

$$\bar{D} = \frac{J_{st}L}{C_h}, \quad \text{from eq. (7)} \tag{31}$$

and $D_\ell = L^2/6t_\ell$, from eq. (11), knowing that eq. (12) is integrated as

$$t_\ell = \frac{L^2}{4D_0} \frac{4e^{\gamma C_h} - 1 + e^{2\gamma C_h}(2\gamma C_h - 3)}{(e^{\gamma C_h} - 1)^3} \tag{32}$$

The measurements, performed again as test Pervaporation no. 2, are completely reproducible (see Table VI). From both tests, the water content should be $C_h = 0.42$ mmol cm^{-3} (≈0.66% w/w) upstream inside the film.

Discussion

Other tests in Table VI were carried out in order to validate the law $D = D_0 e^{\gamma C}$. The test Pervaporation no. 3 concerns pervaporation with lower water activity ($a_h = 0.58$) by using a saturated NaBr solution. It was expected that C_h and α would decrease and that γ would remain constant. However, the variation of α was negligible, while γ increased more than twofold. It is possible that the high amount of salt in Pervaporation no. 3 could modify the sorption and diffusion of water inside the polymer. For this reason, the study was completed with two permeation tests: Permeation nos. 1 and 2 in Table VI. In this case, the upstream side was filled with humidified nitrogen ($a_h = 0.95$ and $a_h = 0.58$). It was decided not to reach 100% RH (or $a_h = 1$) as this is impossible without causing water condensation. Pervaporation no. 1 or 2 and Permeation no. 1 ($a_h = 1$ and 0.95) show quite similar values of permeability (P), plasticization (γ), and diffusion (e.g.) coefficients. However, a slight difference is observed between liquid and vapor water permeabilities which, apart from the activity ($a_h = 1$ and 0.95), could be attributed to a solubility effect. A phenomenon of the low uptake of penetrants into the polymer from the vapor versus the liquid phase, noticed for a wide variety of polymers/solvents, is known as Schroeder's paradox.[11,12] In the present case, this difference is too low to be really representative of the phenomenon.

The use of permeation was thus justified in order to show the effect of a drop in water activity, and to complete the study, it was essential to extend the trends observed to pervaporation tests. Permeation no. 2 ($a_h = 0.58$) compared to Permeation no. 1 ($a_h = 0.95$) shows a negligible variation of α and a sizable increase of γ. It now seems established that D is time-dependent; this is linked to such phenomena as the kinetics of water association on hydrophilic sites (e.g., —COOH or —OH end groups) and/or to a slow change in the polymer structure due to the water sorption.

CONCLUSIONS

In this work, relative to permeation, we have not only determined the stationary flux through a polymer film, but also analyzed the transient step. The typical curve $J = f(t)$ increases up to the stationary flux J_{st} and has an inflexion point close to a point $R(t_R, J_R)$ for which $J_R = 0.24J_{st}$. Near R, the curve is practically linear and its slope becomes maximum. In addition to J_{st} and t_R from which the permeability coefficient P and a diffusion coefficient D_R are calculated, the slope α at the point R, and in a reduced scale, could account for a variation of the diffusion coefficient D during the permeation process.

In numerous cases, the value of α could be sufficient to obtain the law of variation of D, which is often limited to a concentration depen-

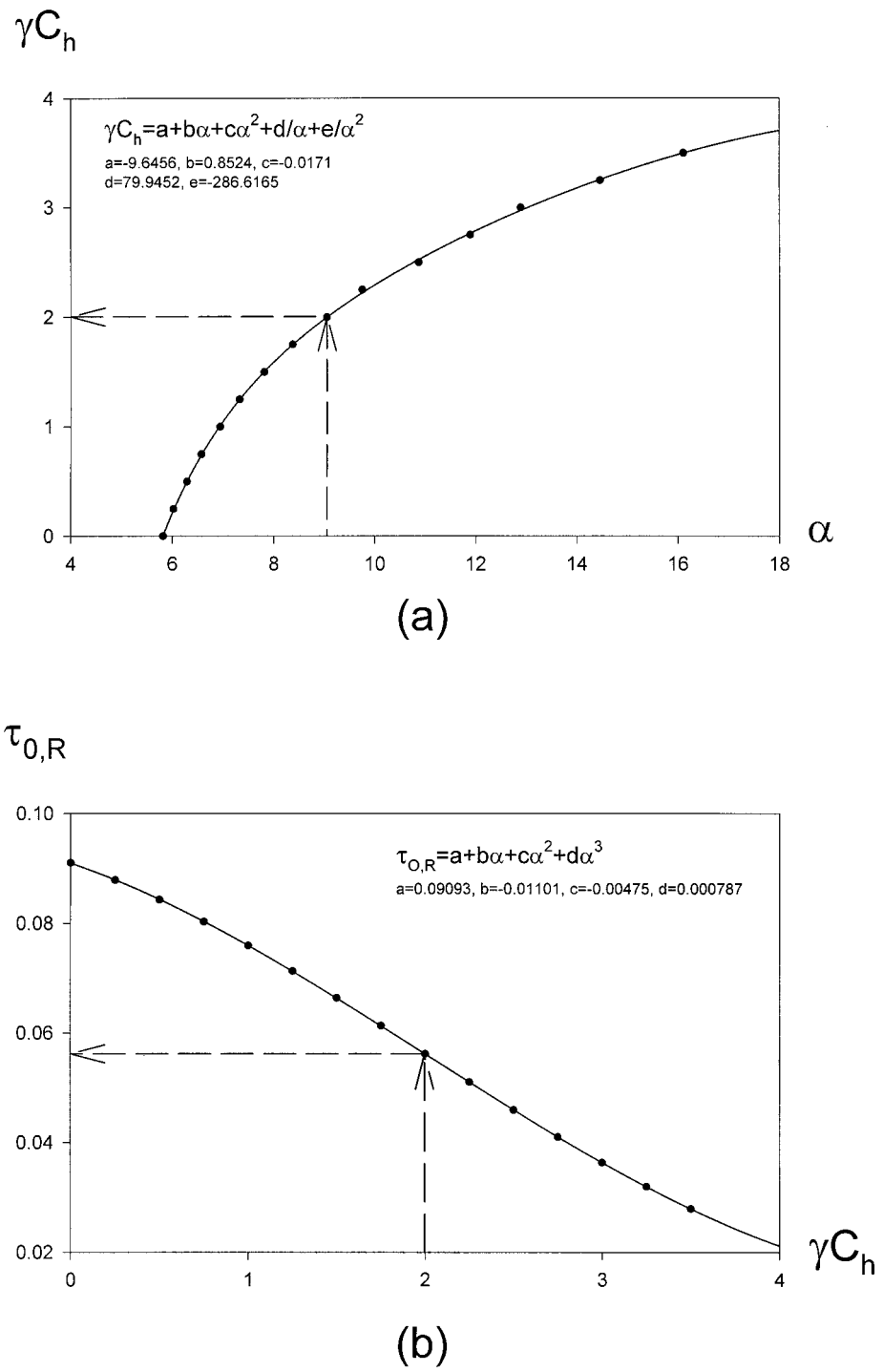

Figure 8 Relations between C_h and the slope (a) γ or (b) $\tau_{0,R}$ in accordance with figures 4(a,b).

dence of type $D = D_0(1 + \beta C)$ or $D = D_0 e^{\gamma C} \ldots$, with only one parameter β or $\gamma \ldots$ to be fitted. Thus, a theoretical curve can be computed and compared with the experimental data as a preliminary proof of the selected law. Additional tests for various upstream activities can be carried out in order to confirm the good agreement. This method could be especially suited to the rubbery polymers. Here, the diffusion of water through a UPR film, a glassy polymer, has been studied

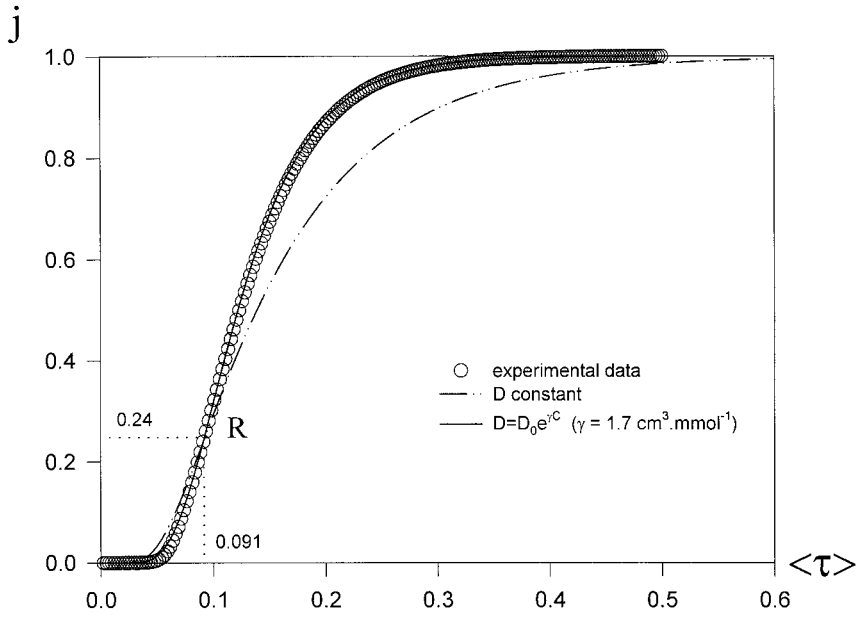

Figure 9 Flux j versus time $<\tau>$ see eqs. (15) and (27) (reduced scales). Comparison between experimental data and simulated curves with D = constant and $\gamma = D_0 e^{\gamma C}$ and $\gamma C_h = 1.7$.

with a permeameter developed in our laboratory. The rate of water transfer rose by between 2 and 4 g of water per square meter per day (film 0.028-cm thick) while the transient flux $J = f(t)$ was recorded with a high accuracy. The diffusion coefficient increased during the permeation process and, at first, this was attributed to an exponential dependence of D on the concentration. However, a more thorough study has shown a time-dependence of D. It could be that the sorption of water at the film interface is not as fast as might be assumed from a quasi-instantaneous local equilibrium. Moreover, the sorption of water could be at the origin of a slow relaxation of the polymer. A complementary study of the kinetics and equilibria of sorption would contribute to a better interpretation of the diffusion coefficient variation.

SYMBOLS, ABBREVIATIONS, AND UNITS

a_h	water activity (= 1 in pervaporation, = p_h/p_{st} in permeation)
$C(x,t)$	concentration of water inside the polymer (mmol cm^{-3})
C_h	upstream concentration (x = 0)
$\bar{D}$	integral diffusion coefficient (cm^2 s^{-1})
D_R	diffusion coefficient constant (= 0.091 L^2/t_R, cm^2 s^{-1})
D_ℓ	diffusion coefficient from time lag (= $L^2/6\ t_\ell$ cm^2 s^{-1})
D_0	diffusion coefficient at C = 0 (x = L) (cm^2 s^{-1})
D_M	diffusion coefficient at $C = C_h$ (x = 0) (cm^2 s^{-1})
f	flow rate of the sweeping gas (= 9.3 cm^3 s^{-1})
$J(x,t)$	flux at position x of the film and at time t (mmol cm^{-2} s^{-1})
$J(L,t)$	downstream flux (x = L) (mmol cm^{-2} s^{-1})
J_{st}	flux in steady state (mmol cm^{-2} s^{-1})
j	reduced flux(J/J_{st})
L	thickness of the polymer film (= 0.0278 cm)
P	permeability coefficient (mmol cm^{-1} s^{-1})
p_h	upstream vapor pressure
p_{st}	saturated vapor pressure
Q	water quantity accumulated in receiving (downstream) chamber (mmol)
S	surface exposed to diffusion (= 30 cm^2)
T_{dp}	dew point temperature (K)
t_l	time lag (= $L^2/6D$) (s)

γ	plasticization coefficient($cm^3\ mmol^{-1}$)
σ	solubility coefficient ($mmol\ cm^{-3}$)
$<\tau>$, τ_0, $\tau_{0,R}$, τ_R	reduced times.

REFERENCES

1. Asbee, K. H. G.; Frank, F. C.; Wyatt, R. C. Proc R Soc (A) 1967, 300, 415.
2. Métayer, M.; Labbé, M.; Marais, S.; Langevin, D.; Chappey, C.; Dreux, F.; Brainville, M.; Belliard, P. Polym Test, in press.
3. Carslaw, H. S.; Jaeger, J. S. Conduction of Heat in Solid, 2nd ed.; Oxford Press: Oxford, 1959; p 308. Crank, J.; Park, G. S. Diffusion in Polymers; Academic: London, New York, 1968; Chapter 1.
4. Frisch, H. L. J Polym Sci 1957, 61, 93.
5. Data from American Institute of Physics Handbook, 3rd ed.; McGraw-Hill: New York, 1989.
6. Equation 8092 [AsymSigR] from Jandel Scientific, Table Curve 2D; Windows version 2.02; AISN Software, 1984–1994.
7. Prager, S.; Long, F. A. J Am Chem Soc 1951, 73, 4072.
8. Zolandz, R. R.; Fleming, G. K. II/Gaz Permeation; Membrane Handbook; Van Nostrand Reinhold: New York, 1992; p 31.
9. Marais, S.; Métayer, M.; Labbé, M.; Legras, M. T.; Saiter, J. M. Polym Eng Sci, in press.
10. Crank, J. The Mathematics of Diffusion; Oxford Press: Oxford, 1975.
11. Schroeder, P. Z Phys Chem 1903, 45, 75.
12. Zawodzinski, T. A., Jr.; Derouin, C.; Radzinski, S.; Sherman, R. J.; Smith, V. T.; Springer, T. E.; Gottesfield, S. J Electrochem Soc 1993, 140, 1042.